JMEPEG (2010) 19:1344–1351
DOI: 10.1007/s11665-010-9624-2

1059-9495/$19.00

Processing and Composition Effects on the Fracture Behavior of Spray-Formed 7XXX Series Al Alloys

M.M. Sharma, C.W. Ziemian, and T.J. Eden

(Submitted August 4, 2009; in revised form January 5, 2010)

The fracture properties of high-strength spray-formed Al alloys were investigated, with consideration of the effects of elemental additions such as zinc, manganese, and chromium and the influence of the addition of SiC particulate. Fracture resistance values between 13.6 and 25.6 MPa $(m)^{1/2}$ were obtained for the monolithic alloys in the T6 and T7 conditions, respectively. The alloys with SiC particulate compared well and achieved fracture resistance values between 18.7 and 25.6 MPa $(m)^{1/2}$. The spray-formed materials exhibited a loss in fracture resistance (K_I) compared to ingot metallurgy 7075 alloys but had an improved performance compared to high-solute powder metallurgy alloys of similar composition. Characterization of the fracture surfaces indicated a predominantly intergranular decohesion, possibly facilitated by the presence of incoherent particles at the grain boundary regions and by the large strength differential between the matrix and precipitate zone. It is believed that at the slip band-grain boundary intersection, particularly in the presence of large dispersoids and/or inclusions, microvoid nucleation would be significantly enhanced. Differences in fracture surfaces between the alloys in the T6 and T7 condition were observed and are attributed to inhomogeneous slip distribution, which results in strain localization at grain boundaries. The best overall combination of fracture resistance properties were obtained for alloys with minimum amounts of chromium and manganese additions.

Keywords aluminum, electron microscopy, failure analysis, mechanical testing, metal matrix composites

1. Introduction

The 7XXX series alloys have been widely used in structural applications due to their high strength-to-weight ratio and excellent mechanical properties (Ref 1). As a result of their demand in this regard, a lot of research has been focused on improving the room temperature fracture properties of these materials. The ingot metallurgy (IM) alloys of the 7XXX series exhibit several disadvantages, including coarse grains and macrosegregation that result in low fracture toughness. Additional shortcomings due to the inherent production process include coarse intermetallic constituent phases and solid solubility limitations. Processes that incorporate high cooling rates, such as powder metallurgy (PM), have been used to improve on these weaknesses and produce alloys possessing fine, segregation-free microstructures, which can be stabilized further during post-processing techniques, such as hot rolling or forging. A significant limitation associated with the PM process, however, is the formation of fracture-inducing oxides on the powder surface (Ref 2, 3). Processing by spray metal forming alleviates this problem by incorporating the powder atomization and consolidation into a single step in an inert atmosphere. The spray metal forming process successfully reduces the oxide content substantially, and thereby increases ductility (Ref 4, 5). As a result of this and other apparent benefits, the spray forming process has received considerable attention as an alternative method for the synthesis of a variety of structural materials (Ref 6), and has been used for this study.

The requirements for high yield stress and good fracture toughness are known to be contradictory (Ref 7, 8), and have hampered the extensive development and utilization of high-strength 7XXX series aluminum alloys. The 7075 alloy for instance, while widely used, suffers from limitations including quench sensitivity (a reduction in the age-hardening capacity due to low quench rates) (Ref 9), susceptibility to stress corrosion cracking (SCC) in the T6 temper, and deterioration of strength in thick sections of the plate (Ref 10). A few of these limitations are overcome with the 7050 alloy, which relies on Zr rather than Cr for grain size control and a subsequent reduction in the quench sensitivity (Ref 4, 9, 10). The 7050 alloy also has reduced amounts of Fe and Si to raise fracture toughness (Ref 9) and increase the fatigue crack growth resistance (Ref 11), and increased ratios of Zn/Mg and Cu/Mg to improve SCC and provide additional strengthening. Control over Fe and Si contents and other impurities is important due to their low solid solubilities in aluminum and their tendency to readily combine with other elements to form large constituent particles known to impair ductility, fracture resistance, and reduce strength (Ref 12). Highly alloyed compositions of the 7XXX series and variations thereof have been developed utilizing the addition of specific transition metals. These additions of trace elements lower solubility and diffusivity of solute in the matrix, thereby reducing precipitate coarsening and thus extending the thermal stability of the alloys (Ref 13). These highly alloyed

M.M. Sharma and **C.W. Ziemian**, Department of Mechanical Engineering, Bucknell University, Dana Building, PO Box A0551, Lewisburg, PA 17837; and **T.J. Eden**, Applied Research Laboratory, The Pennsylvania State University, P.O. Box 30, N. Atherton St, State College, PA 16804-0030. Contact e-mail: msharjud@bucknell.edu.

compositions show great promise toward the optimization of 7XXX series alloys.

While the development of high-strength 7XXX alloys has been successful, further enhancement of their properties is sought by the addition of a high volume fraction of a whisker or particulate carbide. Metallic materials reinforced with brittle fibers, whiskers, or particulates (metal matrix composites or MMCs) have been shown to provide desirable mechanical properties including improved specific stiffness, plastic flow strength, creep resistance, and corrosion resistance (Ref 14). More specifically, the addition of refractory SiC fiber, particulate, and/or whisker to aluminum matrices has been associated with an increase in strength, modulus, and wear resistance. Although a reduction in ductility and fracture toughness typically accompanies these improvements in properties, the significant increase in modulus, often up to 50%, continues to be the motivation behind the addition of high volume fraction carbides to these alloys. A compromise is required in the volume fraction, size, and distribution of the reinforcement phase to achieve an effective structural alloy. To achieve a reasonable balance of strength, modulus, fracture toughness, and ductility, a limit of 20 vol.% is considered for carbide reinforcements.

Although the addition of SiC is usually accompanied by an increase in strength, this is not always the case. Hildman and Koczak (Ref 2), Lewis and Davinroy (Ref 5), and Vaidya et al. (Ref 15) evaluated spray-formed 8090 alloy with additions of 13 and 15 vol.% SiC_p, respectively. While Vaidya et al. (Ref 15) observed marginal increases in strength over unreinforced 8090, Lewis and Davinroy (Ref 5) found similar strengths; and Hildman and Koczak (Ref 2) noted decreased tensile strength compared to monolithic spray-formed 8090. All researchers found that the presence of SiC particulate increased the stiffness and decreased the tensile ductility in their spray-formed 8090 + SiC alloys compared to monolithic 8090. Other investigators (Ref 16, 17), who studied the effect of SiC_p on 7075 and Al-Zn-Mg alloys, observed superior mechanical properties (not including elongation to failure) compared to monolithic alloys.

This study was undertaken to provide insight into the effects of zinc, copper, manganese, and chromium content, as well as the addition of ceramic SiC particle reinforcement, on the fracture properties of spray-formed high-strength aluminum alloys. This article presents results of comparative fracture mechanics tests on Al-Zn-Mg-Cu alloys of different chemical composition and heat treatments, including MMCs reinforced with ceramic SiC particles. The overarching goal of the study is to characterize the fracture toughness and related mechanics behavior of rapidly solidified ultra-high-strength alloys, with a focus on critical variables affecting damage tolerance properties.

2. Experimental Procedure

Two base alloys were selected to be the focus of this investigation, with compositions of 9Zn-1.3Cu-0.34Mn-0.22Cr and 8Zn-1.6Cu-3.97Mn-0.4Ag. The alloy compositions were then varied to study the effects of zinc, copper, manganese, chromium, and silver content on the mechanical properties. SiC particulate was also added to alloys with compositions similar to the unreinforced alloys. A total of seven 7XXX series alloys, including four monolithic and three reinforced (containing 12 to 15 vol.% SiC particulate), were studied in this investigation. Table 1 displays the chemical composition and designation of these seven alloys.

The alloys were all prepared by spray metal forming, or the Osprey process. The details of this process are described elsewhere (Ref 10). In this particular experiment, the spray deposition involved the atomization of the molten metal by nitrogen at 850 to 1000 °C. The gas-to-metal ratio was 4.45 cubic meters of atomized gas per kilogram of metal atomized (Ref 20-22). After the billets were sprayed, they were each hot extruded at 400 °C into a round rod at an extrusion ratio of 44:1. Alloys were then solution treated between 470 and 490 °C for 0.5 to 2 h, quenched in cold water, and then artificially aged to a T6 and T7 temper.

Due to the size of the extruded bars used in this study, fracture toughness testing was conducted using short rod specimens rather than compact tension (CT) tests or single-edge-notch bend tests. Each specimen was first turned down on a lathe from the extruded 28.58 mm diameter to a 25.40 mm diameter $\pm$ 0.0254 mm. Using ASTM E8-04 (Ref 23) guidelines for tensile testing, specimens were machined with grip diameters of 25.40 mm and gage diameters of 19.0 mm. Sharp V-notches were machined into the center of the gage section of the round bar samples, with a diameter of 13.46 mm. A minimum of five specimens per alloy were generated for fracture toughness testing.

Prepared samples were loaded into an Instron testing machine and a tensile load was applied at a constant rate. Based on the test results, the plane strain fracture toughness, K_I

Table 1 Composition of alloys tested, wt.%

Alloy designation	Zn	Mg	Cu	Mn	Zr
9Zn-1.3Cu-0.34Mn-0.22Cr	9.31	3.49	1.25	0.34	0.25
12Zn-1.1Cu-0.29Mn-0.02Cr	12.00	3.28	1.15	0.29	0.20
12Zn-1.1Cu-0.20Mn-0.16Cr	12.00	3.34	1.12	0.20	0.20
8Zn-1.6Cu-3.97Mn-0.04Ag	8.21	2.78	1.58	3.97	0.42
12Zn-1.1Cu-0.26Mn-0.22Cr + SiC_p	11.69	3.23	0.99	0.26	0.14
11Zn-1.2Cu-0.36Mn-0.16Cr + SiC_p	11.20	2.93	1.21	0.36	0.18
9Zn-1.6Cu-3.27Mn-0.04Ag + SiC_p	9.10	2.78	1.60	3.27	0.45
Eura-1 (Ref 18, 19)	10-13	(a)	(a)	(a)	(a)
Eura-2 (Ref 19)	12.00	3.00	0.90	0.19	0.20

(a) Exact amount unknown

(Ref 24), was computed using Eq 1, where P is the maximum load at failure, D is the diameter of the gage section, and d is the diameter of the sharp V-notch, over the range of $1.2 \leq D/d \leq 2.1$.

$$K_I = 0.932\,P\,(D)^{1/2}/(\pi d^2)^{1/2} \quad \text{(Eq 1)}$$

Fracture surfaces from fracture resistance (K_I) were then examined using scanning electron microscopy.

3. Results and Discussion

3.1 Microstructure

This article is one in a series of articles that deals with separate aspects of the same set of aluminum alloys. A detailed microstructural evaluation of the alloys considered in this study has thus been reported previously (Ref 6, 22, 25, 26). In this previous study, it was determined that the spray-formed alloys contained a variety of solute elements and an increased amount of zinc content as compared to conventional 7XXX series alloys. The characteristic of the T6 spray-formed alloys is predominantly associated with a massive precipitation of the η′ (eta prime) structural particles with the T7 alloys containing the η ($MgZn_2$) phase as well. It was observed that this microstructure is most easily achieved with alloys containing a high amount of solute content, with Zn + Mg contents over 15 wt.% in which the zinc content is at least ~12 wt.%. Furthermore, it was found that a massive and fine distribution of the η′ strengthening phase can also be achieved with lower amounts of Zn and Mg, if accompanied by the addition of manganese and minimum amounts of silver (less than 0.04 wt.%). All alloys contained Al_3Zr dispersoids, which also contributed to the strengthening of the alloys through pinning of grain boundaries (Ref 25). In previous studies (Ref 22, 25), the effect of adding chromium or manganese was found to promote the formation of a rod-like dispersoid, $Al_{18}Cr_2Mg_3$ (E-phase), or the quasi-ternary ($Al_{20}(Cu,Zn)_2Mn_3$) intermediate phase, respectively. Both of these dispersoids contribute a fiber-like reinforcement toward strengthening. Furthermore, large constituent particles identified as $Al_6(MnFe)$ and Al_7Cu_2Fe were found throughout the matrices of the various spray-formed alloys. The size and number of the constituent particles varied in each alloy and correlated with the composition. In addition, the concentration of GP zones, η ($MgZn_2$), and η′ particles increased with increasing solute content. It was concluded that the ultra-high strengths of the spray-formed alloys is attributed to multiple effects of both precipitation hardening and fiber reinforcement.

3.2 Fracture Resistance (K_I)

The results of the fracture resistance tests are shown in Table 2 for the monolithic and MMC materials. Overall fracture resistance values between 18 and 25.6 MPa $(m)^{1/2}$ were obtained in the T6 and T7 conditions. The 8Zn-1.6Cu-3.97Mn-0.04Ag alloy displayed the lowest fracture resistance of 13.6 and 16.8 MPa $(m)^{1/2}$ for the T6 and T7 conditions, respectively. Comparison of the spray-formed alloys in this study with data for IM 7075-T6 (Ref 18) alloys revealed that the spray-formed alloys had considerably lower fracture resistance. IM 7075-T6 has a fracture resistance of ~31 MPa $(m)^{1/2}$, whereas the best performing spray-formed alloy had a fracture resistance of ~25 MPa $(m)^{1/2}$. However, compared to high-solute PM alloys of similar composition in the T6 condition which have a fracture resistance of ~7.3 (Ref 17) and 13 MPa $(m)^{1/2}$ (Ref 19), the spray-formed alloys demonstrated significantly improved fracture resistance. The loss of fracture resistance compared to IM 7075-T6 was unanticipated based on results from a previous study which showed the spray-formed alloys to have improved tensile properties over the conventional alloys (Ref 6, 22, 25). The obtained values for fracture toughness and elongation were overall more closely comparable to the Eura (Ref 19) spray-formed alloys, with the exception of the 12Zn-1.1Cu-0.20Mn-0.16Cr-T7, which exhibited slightly improved fracture resistance. It should be noted that the fracture resistance values (Ref 18, 19) for the Eura alloys were obtained on CT specimen following the ASTM E-399 standard practice, as opposed to

Table 2 Fracture Properties of Tested Alloys

Alloy Designation	Condition	Elongation, %	Elastic modulus, GPa	Fracture resistance, MPa $(m)^{1/2}$
9Zn-1.3Cu-0.34Mn-0.22Cr	T6	6.0	61.4	20.0
	T7	5.4	60.7	18.0
12Zn-1.1Cu-0.29Mn-0.02Cr	T6	4.5	71.0	22.0
	T7	5.3	72.4	23.1
12Zn-1.1Cu-0.20Mn-0.16Cr	T6	6.5	67.6	22.5
	T7	5.4	65.5	25.6
8Zn-1.6Cu-3.97Mn-0.04Ag	T6	3.8	70.3	13.6
	T7	3.3	68.3	16.8
Eura-1 (Ref 18, 19)	T6	4.9	···	17.0
	T7	5.4	···	23.8
Eura-1 (Ref 18, 19)	T6	2.2	···	15.0
	T7	5.4	···	23.8
Eura-2 (Ref 18)	T6	7.1	···	23.2
12Zn-1.1Cu-0.26Mn-0.22Cr + SiC_p	T6	4.4	91.0	20.3
	T7	4.3	95.2	25.6
11Zn-1.2Cu-0.36Mn-0.16Cr + SiC_p	T6	4.7	88.3	18.7
	T7	4.4	84.8	17.9
9Zn-1.6Cu-3.27Mn-0.04Ag + SiC_p	T6	1.9	99.3	19.9
	T7	1.5	98.6	21.3

notched round bar used in this study. Fracture resistance values of the MMC materials compared well with unreinforced counterparts.

The elastic modulus of MMC alloys increased by approximately 40%, from an average of 66.4 to 92.9 GPa, when compared to monolithic alloys of similar compositions. As expected, the addition of particulate reinforcement was detrimental to the ductility of the alloys, which decreased by up to 50 and 54% for the T6 and T7 conditions, respectively, in the alloys with silver and high manganese, and by up to 44 and 20% for the T6 and T7 conditions, respectively, for alloys without silver.

The balance of properties is reasonably good with the addition of SiC particulate, despite the decreases in ductility. The overall combination of fracture properties achieved with the SiC-reinforced alloys is advantageous for a number of potential structural applications. In fact, the values achieved in this study are significantly better than those of Komai et al. (Ref 16), who obtained elongation to failure less than 2% with concomitant tensile and yield strengths of 844 and 740 MPa, respectively, in PM-processed 7075 SiC whisker-reinforced alloys.

3.3 Fractography

It has been documented (Ref 27) that high-strength aluminum alloys fail by either one or a combination of two mechanisms, void growth and eventual void coalescence, which occurs by the mechanisms of void sheet formation or void impingement (Ref 28). To identify the possible mechanisms for rupture in this study, evidence for the critical features on the fracture surfaces of the alloys was sought. Particular attention was given to identify the differences in fracture surface between the alloys with varying heat treatment. First, a quantitative microstructural analysis of the large constituent particles was conducted (Table 3). The results were similar for both the T6 and T7 conditions, since aging condition does not affect large constituent initiation or growth (Ref 15, 26). It was observed that as the size and volume fraction of large second phase constituent particles increased, the interparticle spacing decreased. The fracture behavior in the spray-formed alloys is believed to be associated with the volume fraction, size, and spacing of large second phase particles. This is discussed in more detail later in this article.

3.3.1 Observations of Alloys in the T6 Condition. Fracture morphologies of the spray-formed alloys in the T6 condition were characterized by ductile transgranular rupture, with a component of intergranular fracture and secondary cracking (Fig. 1). For the most part, microshearing along slip lines was observed (Fig. 1a). The width of the sheared area is the magnitude of the grain size, and the elongated shape of the grains is clearly visible (Fig. 1b). Microshearing is believed to be attributed to the slip behavior of these alloys; in the T6 temper, the hardening particles are composed mainly of η′ precipitates (Ref 6, 22, 25); as a result, these semicoherent/coherent particles can be cut by dislocations (Ref 29). This behavior implies planar slip, in combination with high strain concentrations along the slip bands (Ref 4). Thus, when a critical strain is exceeded, failure by shearing along the slip bands will occur. Further investigation found grain faceting associated with microvoids to be apparent (Fig. 2). In the high-zinc (>9% Zn) alloys, the fracture surface was characterized by a predominantly intergranular fracture (Fig. 3). An intergranular fracture is associated with the growth or increased number of precipitates at the grain boundary (Ref 30, 31). Grain boundary precipitates were observed in these alloys in previous studies (Ref 22, 25, 26) and were identified to be η′ hardening plates. In the 8Zn-1.6Cu-3.97Mn-0.04Ag alloy, the fracture surface was noticeably different than the other T6 alloy microstructures. Due to the very high solute content from increased amount of manganese and additions of silver, larger constituent particles are observed still located at the fracture surface (Fig. 4). The majority of the particles is not cracked and are still intact at the fracture surface. As seen with the other spray-formed alloys, fracture is predominantly intergranular.

3.3.2 Observations of Alloys in the T7 Condition. In a previous related study (Ref 22), the microstructure of the spray-formed alloys in the T7 condition was thoroughly characterized. It was found that the majority of the hardening particles

Table 3 Quantitative analysis of the constituent particles larger than 1 μm

Alloy designation	V_f, %	Size range, mm	Spacing, mm
9Zn-1.3Cu-0.34Mn-0.22Cr	2.5	0.5-2	13
12Zn-1.1Cu-0.29Mn-0.02Cr	1.2	0.5-1	13
12Zn-1.1Cu-0.20Mn-0.16Cr	1.5	0.1-0.75	15
8Zn-1.6Cu-3.97Mn-0.04Ag	4.5	0.5-5	2

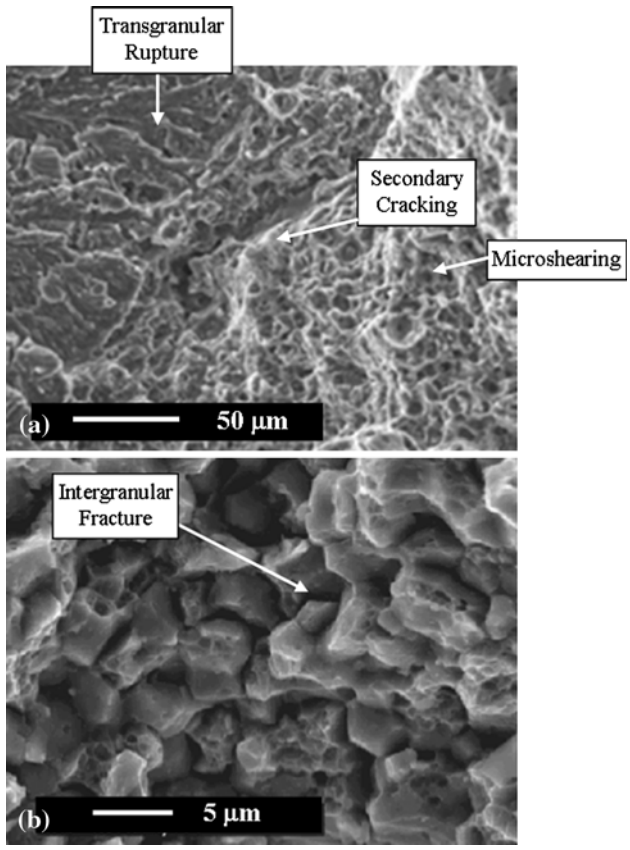

Fig. 1 Fracture surface of a 9Zn-1.3Cu-0.34Mn-0.22Cr-T6 alloy showing the varying fracture morphology: (a) low magnification and (b) high magnification

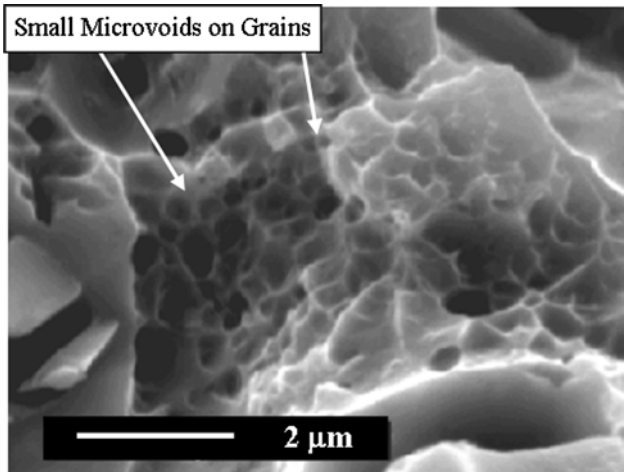

Fig. 2 Scanning electron micrograph of fracture surface of a 9Zn-1.3Cu-0.34Mn-0.22Cr-T6 alloy showing small microvoids associated with fracture

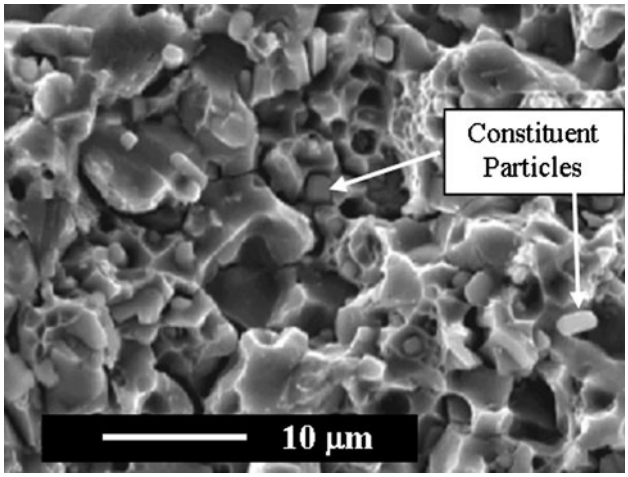

Fig. 4 Scanning electron micrograph of fracture surface of a 8Zn-1.6Cu-3.97Mn-0.04Ag-T6 alloy. Note the number and distribution of constituent particles that are still present at the fracture surface

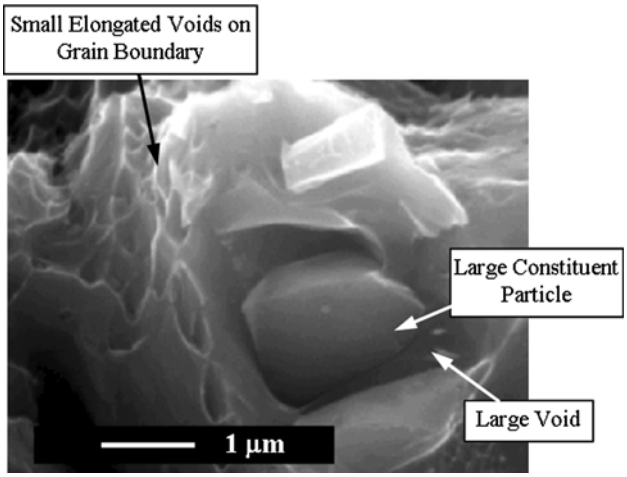

Fig. 3 Scanning electron micrograph of fracture surface of a 12Zn-1.1Cu-0.20Mn-0.16Cr-T6 alloy near a grain boundary. Note the two different void sizes; small elongated voids from fine precipitates and a large void from a dispersoid constituent particle

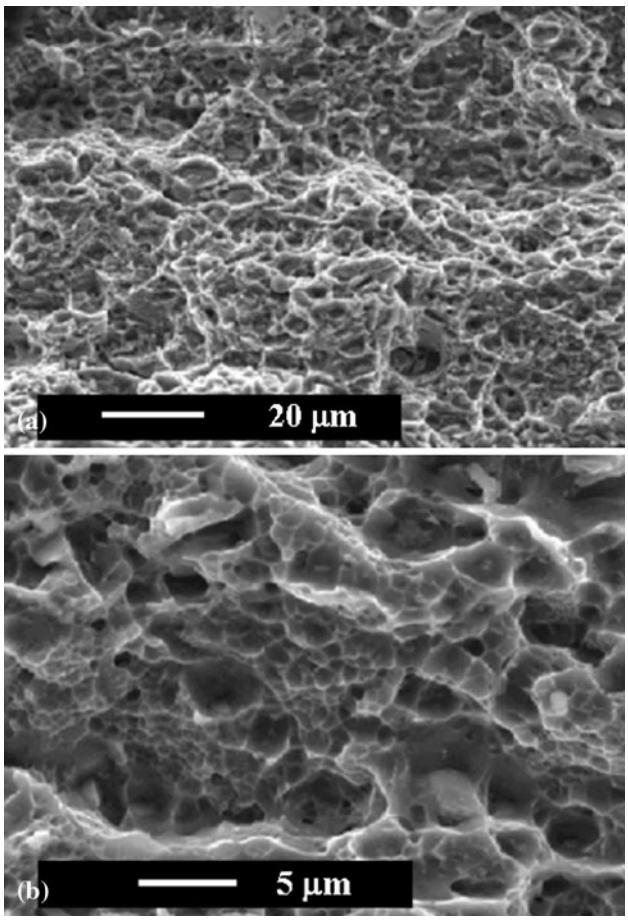

Fig. 5 Scanning electron micrograph of fracture surface of a 12Zn-1.1Cu-0.20Mn-0.16Cr-T7 alloy showing the varying fracture morphology of ductile dimple fracture at (a) low magnification and (b) microvoids at high magnification

are η′ plates; however, a significant amount of η($MgZn_2$) precipitates are also observed in the overaged condition. These η($MgZn_2$) precipitates are incoherent and, thus, cannot be cut by dislocations (Ref 29). This predominant microstructure implies homogeneous slip, which results in a change in fracture mode from microshearing to ductile dimple fracture when comparing T6 and T7 heat treatments (Fig. 5a, b). It was observed that the dimple spacing is frequently larger than the particle spacing, signifying that voids formed only at a fraction of the intermediate particles in the path of the crack. The fracture surfaces were characterized by a bimodal distribution of equiaxed voids (Fig. 5b). Through the use of EDAX and microprobe elemental analysis, it was found that large voids nucleated around Al_6(MnFe) or Al_7Cu_2Fe constituent particles, while the small dimples were associated with the smaller, more fine, dispersoids (Al_3Zr, or the E-phase) (Ref 22). The EDAX results are presented in Fig. 6(a) and (b). These phases were identified in a previous study (Ref 22) and found to exist in the spray-formed alloys. In explaining why only some voids formed at particles, it has been reported (Ref 32, 33) that large voids first evolve through nucleation from cracking of large

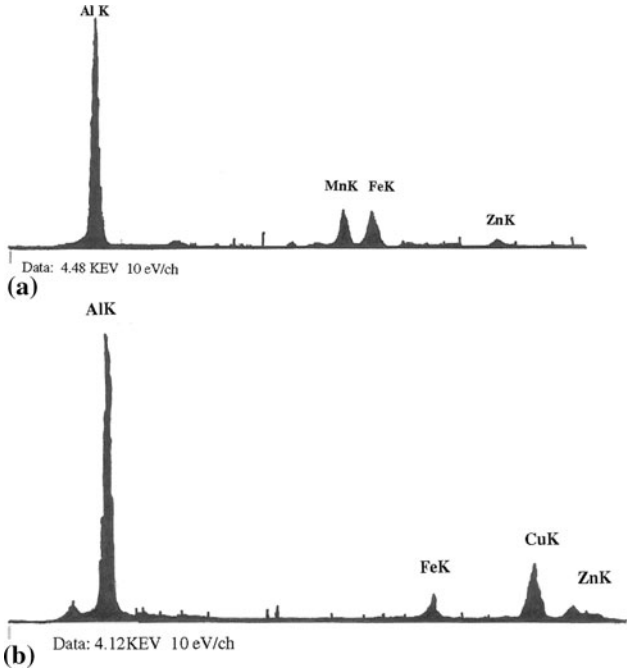

Fig. 6 Energy-dispersive X-ray analysis (EDAX) results of (a) $Al_6(MnFe)$ and (b) Al_7Cu_2Fe constituent particles

second phase particles (1 to 10 μm). Larger particles will crack at lower strains. The stress necessary to initiate particle cracking is proportional to $D^{-1/2}$, where D is the average particle diameter in the plane normal to the largest principal stress (Ref 32, 33). After continuous deformation, the faces of the cracked particles separate. This action results in a void, which grows in the matrix. The extent to which the void grows is dependent on the increasing spacing-to-size ratio of the void-nucleating particles. This mechanism can be related to the spray-formed alloys in this study. The alloy with the largest spacing-to-size ratio (12Zn-1.1Cu-0.20Mn-0.16Cr) had the best fracture resistance, while the 8Zn-1.6Cu-3.97Mn-0.04Ag alloy had the worst fracture resistance and the smallest spacing-to-size ratio. This can be further explained by stating that the close spacing of precipitates and particles creates a short mean link up distance for void growth and coalescence. Thus, crack or void growth will be enhanced when interparticle spacing is decreased. This deleterious effect on fracture resistance in high-strength, high-solute 7XXX series alloys has been noted by several researchers (Ref 18, 19, 34-36).

Ludka and Laughlin (Ref 30) observed fracture morphologies comparable to those in this study, in conventionally processed high-strength aluminum alloys tested under related conditions. They noted a drastic decrease in toughness and a concomitant transition in the fracture mode (from transgranular to intergranular dimpled ruptures) when going from a low solute (σ_{YS} = 496 MPa, σ_{UTS} = 551 MPa) to high solute (σ_{YS} = 614, σ_{UTS} = 654 MPa) content. In addition, it was observed that in high-solute alloys the slip character is much coarser than in low-solute alloys; therefore, slip bands have larger offsets associated with them. This observation concurred with predictions of a work-softening model developed by Hornbogen and Zum Gahr (Ref 31). Furthermore, Ludka and Laughlin (Ref 30) noted that, in ultra-high-strength materials, the strength differential between the matrix and the precipitate free zone, $\sigma_M - \sigma_{PFZ}$, can be very large and, therefore, the imposed deformations are preferentially dissipated within the soft PFZ regions close to the grain boundaries.

Under the circumstances mentioned above, there is much stronger strain localization at the grain boundaries for the spray-formed aluminum alloys in a given macroscopic strain level. It is believed that at the slip band-grain boundary intersection, particularly in the presence of large dispersoids and/or inclusions, microvoid nucleation would be significantly enhanced. Inhomogeneous slip distribution results in strain localization at grain boundaries, which often results in the occurrence of concomitant intergranular decohesion. This behavior can be further explained by considering the step by step sequence of fracture events that occur during failure in ultra-high-strength spray-formed alloys. Due to the strain localization at grain boundary regions, intergranular cracks form at the intersection of coarse slip bands with grain boundary particles, and longitudinal cracks can propagate under the action of the σ_3 stress. When this occurs, grains are released from their mutual constraints. The unconstrained grains subsequently deform like precipitation-hardened single crystals. Necking and shearing with rotation of the grain boundary inwards takes place until the final ductile rupture of grain interiors occurs (Ref 30). Microstructural observations in this study strongly support the fracture mechanism discussed by Ludka and Laughlin (Ref 30), who use a schematic to illustrate the sequence of events that occur during failure of high-solute alloys. Such a fracture mechanism explains the fracture appearances observed in this study, as well as the concomitant loss in fracture resistance of the spray-formed alloys. The fracture surfaces of alloys with higher chromium and manganese additions were characterized by a large amount of intergranular decohesion and by the presence of fissures (Fig. 7a). The grains were to a great extent, unlinked along their boundaries, exhibit ductile fracture in the central part of the grains (Fig. 7b). The fracture surfaces of the alloys with a decreased amount of chromium and manganese exhibited similar features, although the amount of intergranular decohesion was significantly decreased (Fig. 7c) as well as the depth of fissures (Fig. 7d).

In the ultra-high-strength spray-formed alloys, the weakest parts of the structure are the grain boundary regions (Ref 18, 22, 25). Therefore, a significant improvement in fracture resistance would be attained with the reduction of strain localization (more homogenous deformation within the grains) and by the reduction of large dispersoids and second phase particles, in the grain boundary area. This said, the improvement in fracture resistance obtained for the overaged materials versus the peak aged can be explained by the more homogenous deformation within the matrix and by the reduction of the strength differential. This can be related more to the difference in concentration of fine second phase strengthening particles for each heat treatment condition versus the larger constituent particles. In both the T6 and T7 conditions, the overall significant improvement in fracture resistance of the 12Zn-1.1Cu-0.20Mn-0.16Cr alloy can be attributed to the reduced presence of incoherent Cr or Mn dispersoids as well as increased size-to-spacing ratio of larger constituent particles compared with the properties of the other alloys (Ref 22). The alloys with high manganese (8Zn-1.6Cu-3.97Mn-0.04Ag and 9Zn-1.6Cu-3.27Mn-0.04Ag + SiC_p) displayed the poorest fracture resistance performance, due to the high amount of second phase particles, specifically, the quasi-ternary phase and the larger incoherent Cu-Mn-rich particles (Ref 22).

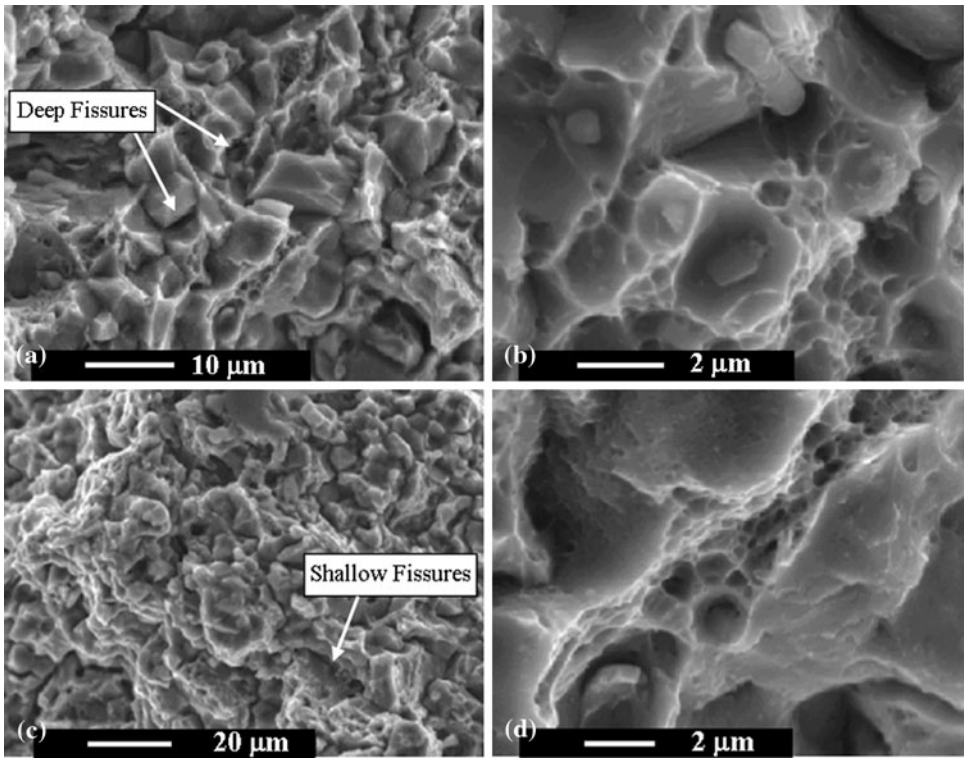

Fig. 7 Scanning electron micrographs of alloys with differing fracture surfaces based on high (9Zn-1.3Cu-0.34Mn-0.22Cr-T6 (a, b)) and low (12Zn-1.1Cu-0.20Mn-0.16Cr-T6 (c, d)) intermetallic content

The fracture process (or processes) in aluminum alloys in this study was essentially by dimpled rupture. From microstructural observations alone, it seems plausible that the dispersoid and constituent particles dominate the fracture mechanisms of the ultra-high-strength alloys. However, based on the fact that a noticeable difference in the fracture properties between alloys in the T6 and T7 conditions was observed, it is believed that structural particles (Ref 25) also play a significant role in the fracture initiation process. Initially, the cracking of large constituent particles nucleates voids, and they eventually manifest as large dimples. The observation relating to the fracture surfaces having two populations of dimples implies that at a later time in the fracture process, nucleation of microvoids is initiated by the decohesion of the dispersoid-matrix interface. These submicron voids constitute sheets of incipient dimples. In the alloys with higher Cu, Mn, and Cr additions, a higher volume fraction of constituent particles (which are substantially larger than the dispersoids) would be expected to nucleate large voids in greater numbers. Statistically, the growth of these voids and their coalescence by mutual impingement are favored in such an instance. In this study, an attempt to obtain specific evidence for void growth and void coalescence was not made. The observation of an increased volume fraction of large-sized second phase particles in higher Cr, Mn, and Cu alloys, however, suggests that a void coalescence mechanism by impingement is operating in the fracture process.

4. Conclusions

The current study is a part of a much larger investigation of spray-formed aluminum alloys that examines the structure/property relationships of the various alloys and the effects of elemental additions. High-solute 7XXX series aluminum alloys were produced by rapid solidification through spray forming. Through variation in manganese and chromium levels and the use of spray parameter optimization, an increase in the interparticle spacing between dispersoid particles was achieved in some alloys, thereby increasing fracture resistance. The damage tolerance of these alloys, however, was not as high as that found in conventional IM 7075-T6, due to the high solute content in the spray-formed alloys but was found to be better than PM-processed alloys of similar composition. In both unreinforced and MMC materials, optimum combined properties were obtained in materials where incoherent Cr- or Mn-rich dispersoids were at a minimum volume fraction and spacing-to-size ratio of dispersoids and constituent particles was high. These microstructures were achieved in alloys with decreased additions of chromium and manganese and increased amounts of Zn (i.e., 12Zn-1.1Cu-.29Mn-0.02Cr, 12Zn-1.1Cu-0.20Mn-0.16Cr and 12Zn-1.1Cu-0.26Mn-0.22Cr + SiC_p). These changes in particle content are believed to have lessened the matrix-dispersoid interface decohesion and thus improved fracture properties.

Fracture morphologies of the spray-formed alloys in the T6 condition were characterized by ductile transgranular rupture, with a component of intergranular fracture and secondary cracking. Fracture morphologies in the T7 condition were characterized by a bimodal distribution of equiaxed voids. It was found that large voids nucleated around Al_7Cu_2Fe or $Al_6(MnFe)$ constituent particles, while the small dimples were associated with the smaller, more fine, dispersoids (Al_3Zr, or the E-phase). Intergranular decohesion appeared to be the final cause of failure in these alloys and is believed to have initiated from slip

band-grain boundary void initiation. The improved fracture resistance of the alloys in the T7 condition is attributed to the homogeneity of deformations within the microstructure and along grain boundaries. The microstructural observations and property trends indicate that it is possible to tailor the manganese and chromium compositions in this alloy system to meet fracture resistance requirements, while keeping the strength high.

Acknowledgments

The authors would like to thank Naval Sea Systems Command for the financial support of this research under contract No. N00039-97-D-0042, Delivery Order Nos. 0214 and 0215

References

1. P. Bai, X. Hou, X. Zhang, C. Zhao, and Y. Xing, Microstructure and Mechanical Properties of a Large Billet of Spray Formed Al–Zn–Mg–Cu Alloy with High Zn Content, *Mater. Sci. Eng. A*, 2009, **508**, p 23–27
2. G.J. Hildeman and M.J. Koczak, Powder-Metallurgy Aluminum Alloys, *Aluminum Alloys—Contemporary Research and Applications*, A.K. Vasudevan and R.D. Doherty, Ed., Academic Press, San Diego, CA, 1989, p 323–364
3. G.N. Grayson, G.B. Schaffer, and J.R. Griffiths, Observations of Oxide Films on Fatigue Fracture Surfaces of a Sintered 2xxx Series Aluminum Alloy, *Mater. Sci. Eng. A*, 2007, **454–455**, p 99–103
4. R. Maechler, P.J. Uggowitzer, C. Solenthaler, R.M. Pedrazzoli, and M.O. Speidel, Structure, Mechanical Properties, and Stress Corrosion Behavior of High Strength Spray Deposited 7000 Series Aluminum Alloy, *Mater. Sci. Technol.*, 1991, **7**(5), p 447–451
5. R.E. Lewis, A.T. Davinroy, and M.J. Kaufman, Microstructural and Property Improvements in 7075 and 8090 Aluminum Alloys by Spray Forming, *Metallurgica*, 1998, **30**, p 185–192
6. M.M. Sharma, M.F. Amateau, and T.J. Eden, Mesoscopic Structure Control of Spray Formed High Strength Al–Zn–Mg–Cu Alloys, *Acta Mater.*, 2005, **53**, p 2919–2924
7. W.-H. Liu, X.-M. Zhang, H.-J. Li, S.-D. Liu, and Z.-B. Huang, Effect of Solution on Fracture Toughness of 7A55 Aluminum Alloy, *J. Central South Univ. Technol.*, 2007, **38**(1), p 1–45
8. K.Y. Lee and O.W. Kim, Stress Intensity Factor for Sheet-Reinforced and Cracked Plate Subjected to Remote Normal Stress, *Eng. Fract. Mech.*, 1998, **61**(3), p 461–466
9. M. Conserva and P. Fiorini, Interpretation of Quench-Sensitivity in Al-Zn-Mg-Cu Alloys, *Metall. Trans.*, 1973, **4**, p 857–862
10. L. Schra and W.G.J. 't Hart, Engineering Property Comparisons of 7050–T73651, 7010–T7651 and 7010–T73651 Aluminium Alloy Plate, *Eng. Fract. Mech.*, 1983, **17**(6), p 493–507
11. M. Zedalis, L. Filler, and M.E. Fine, Effect of Purity and Dispersoid Type on Near Threshold Fatigue Crack Growth Rates in Al-Zn-Mg-Cu Alloys, *Scripta Metall.*, 1982, **16**(4), p 471–474
12. R. Sen, S. Kaiser, M.K. Mitra, and M.K. Banerjee, Plane Strain Fracture Toughness of Scandium Doped Al–6Mg Alloy, *J. Alloys Compd.*, 2008, **457**, p 135–143
13. A.K. Mukhopadhyay and Q.B. Yang, The Influence of Zirconium on the Early Stages of Aging of a Ternary Al-Zn-Mg Alloy, *Acta Metall. Mater.*, 1994, **43**(9), p 3083–3091
14. L. Wang, T. Kobayashi, H. Toda, and M. Hayakawa, Effect of Loading Velocity and Testing Temperature on the Fracture Toughness of a SiCw:6061Al Alloy Composite, *Mater. Sci. Eng. A*, 2000, **280**, p 214–219
15. R.U. Vaidya, Z.R. Xu, X. Li, K.K. Chawla, and A.K. Zurek, Ageing Response and Mechanical Properties of a SiC_p/Al-Li (8090) Composite, *J. Mater. Sci.*, 1994, **29**(11), p 2944–2950
16. K. Komai, K. Minoshima, and H. Ryoson, Tensile and Fatigue Fracture Behavior and Water-Environment Effects in a SiC-Whisker/7075-Aluminum Composite, *Compos. Sci. Technol.*, 1993, **46**, p 59–66
17. J. Faure and B. Dubost, Process for the Production of Aluminum Alloys by Spray Deposition, U.S. Patent 4,995,920, 26 Feb 1991
18. M. DeSanctis and L. Lazzeri, An Evaluation of Fatigue and Fracture Mechanics Properties of Ultra-High Strength 7XXX Series Al-Alloys, *Fatigue Fract. Eng. Mater. Struct.*, 1992, **15**(3), p 249–263
19. M. DeSanctis, Structure and Properties of Rapidly Solidified Ultrahigh Strength Al-Zn-Mg-Cu Alloys Produced by Spray Deposition, *Mater. Sci. Eng. A*, 1991, **141**, p 103–121
20. J.A. Nock and H.Y. Hunsicker, High Strength Aluminum Alloys, *J. Met.*, 1963, **15**(3), p 613
21. M.A. Reynolds and J.G. Harris, Development of a Tough, High-Strength Aluminum Alloy with Improved Stress Corrosion Resistance, *Aluminum*, 1974, **50**, p 592
22. M.M. Sharma, Microstructural and Mechanical Characterization of Various Modified 7XXX Series Spray Formed Alloys, *Mater. Charact.*, 2008, **59**, p 91–99
23. ASTM E8-04," Standard Test Methods for Tension Testing of Metallic Materials," *Book of Standards*, Vol. 3.01, ASTM International, West Conshohocken, PA, www.astm.org
24. H.L. Edwards and R.J.H. Wanhill, *Fracture Mechanics*, Edward Arnold, London, 1984, p 51
25. M.M. Sharma, M.F. Amateau, and T.J. Eden, Hardening Mechanisms of Spray Formed Al-Zn-Mg-Cu Alloys with Scandium and Other Elemental Additions, *J. Alloys Compd.*, 2006, **416**, p 135–142
26. M.M. Sharma, M.F. Amateau, and T.J. Eden, Aging Response of Al-Zn-Mg-Cu Spray Formed Alloys and Their Metal Matrix Composites, *Mater. Sci. Eng. A*, 2006, **424**, p 87–96
27. R.H. VansStone and T.B. Cox, Microscopic Cracking Processes, ASTM STP 600, ASTM, Philadelphia, PA (1976), p 5
28. K. Osamura, H. Okuda, Y. Amemiya, and H. Hashizume, Growth and Coarsening of g. p. Zones in Al-Zn Alloys, *Metall. Mater. Trans. A*, 1988, **19**(8), p 1973–1980
29. V. Gerold and H. Harberkorn, On the Critical Resolved Shear Stress of Solid Solutions Containing Coherent Precipitates, *Phys. Status Solidi*, 1966, **16**, p 675–679
30. G.M. Ludka and D.E. Laughlin, The Effect of Solute Content on the Slip Behavior in 7XXX Series Aluminum Alloys, *Metall. Mater. Trans. A*, 1981, **12**(12), p 1663–1665
31. E. Hornbogen and K.H. Zum Gahr, Distribution of plastic strain in alloys containing small particles, *Metallography*, 1975, **8**, p 181–193
32. J.A. Wagner and R.N. Shenoy, The Effect of Copper, Chromium, and Zirconium on the Microstructure and Mechanical Properties of Al-Zn-Mg-Cu Alloys, *Metall. Mater. Trans. A*, 1991, **22**(11), p 2809–2818
33. R.H. VanStone and J.A. Psioda, Discussion of Metallurgical Factors Affecting Fracture Toughness of Aluminum Alloys, *Metall. Mater. Trans. A*, 1975, **6**(3), p 668–670
34. A.J. Ardell, Precipitation Hardening, *Metall. Trans. A*, 1985, **16**, p 2131
35. A. Wilm, Physikalisch-metallurgische Untersuchungen über magnesiumhaltige Aluminiumlegierungen, *Metallurgie*, 1911, **8**, p 225–227, in German
36. J. Auld and S.M. Cousland, The Transition Phase η′ in Al-Zn-Mg Alloys, *Scripta Metall.*, 1971, **5**(9), p 765–769